The positive history of an error. Modelling the heave of a nuclear power station

Eduardo Alonso

Civil Engineering School. Universitat Politècnica de Catalunya. 08034 Barcelona, Spain

Abstract. The paper describes two different procedures to explain and to model the observed heave of a nuclear power plant founded on an expansive unsaturated claystone. In the initial model developed, the claystone was represented by a double structure (micro-macro) expansive clay. Field swelling records were accurately reproduced and the model was used to predict the long-term (40 yr) expected vertical displacements. Years after, it was realized that a more consistent explanation for the observed heave was the precipitation of gypsum crystals in discontinuities. The alternative physical phenomenon led to a re-formulation of an appropriate model, which is described in the paper. The key aspect of the long-term heave was the presence of anhydrite in the claystone mineralogical composition. The paper explains the physics of crystal growth that was triggered by the construction of the power station, the large excavation performed to locate the plant buildings and by the presence of a phreatic level, that was a consequence of the geometry of excavations. The new model, substantially more complex than the first one, is also able to reproduce available laboratory long-term swelling tests and field observations. It is hopefully a more reliable model to predict the long-term behaviour. The positive part of this history is that the initial model inspired the development of successful elastoplastic constitutive models for expansive clays.

1 Introduction

The construction of the Ascó II nuclear power plant involved a large excavation of a valley slope of the Ebro river, with the purpose of creating a horizontal platform to operate the installation. The foundation material is a firm reddish claystone of Eocene age, horizontally layered (Figs. 1 and 2). The thickness of strata ranges between 1 and 3 m. This claystone is commonly found in the south-eastern region of the large Ebro basin.

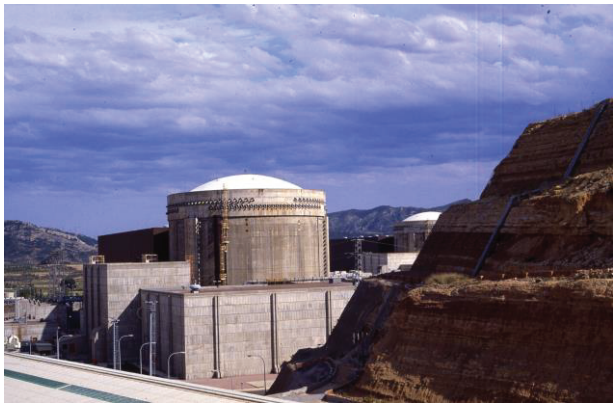

Fig. 1. Containment building and excavated slope in the expansive claystone.

The elevation of the contact rock-foundation slab of the different buildings of the power plant was not constant. This is shown in Figure 2. The excavation created a large "trough" in the claystone that was difficult to drain. Eventually, a phreatic level established in the excavated area.

Figure 3 shows the depth of excavation and the position of the buildings. The maximum depth affects the large "Auxiliary" building, next to the Containment structure.

Heave displacements of buildings were noticed during construction of the installation, at an early time (1976). Levelling marks in all the buildings provided continuous time records of vertical displacements. This information was interpreted periodically to establish the pattern of time and space development of heave. Figure 3 shows measured heave contours in the period 1971 – 2001. The stiffness of the building structures could be identified in this plot.

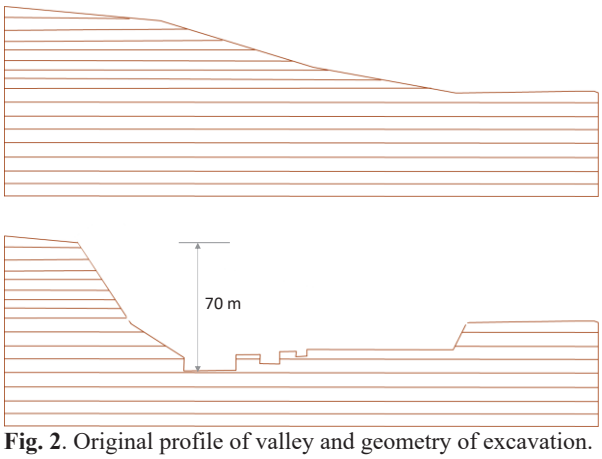

Fig. 2. Original profile of valley and geometry of excavation.

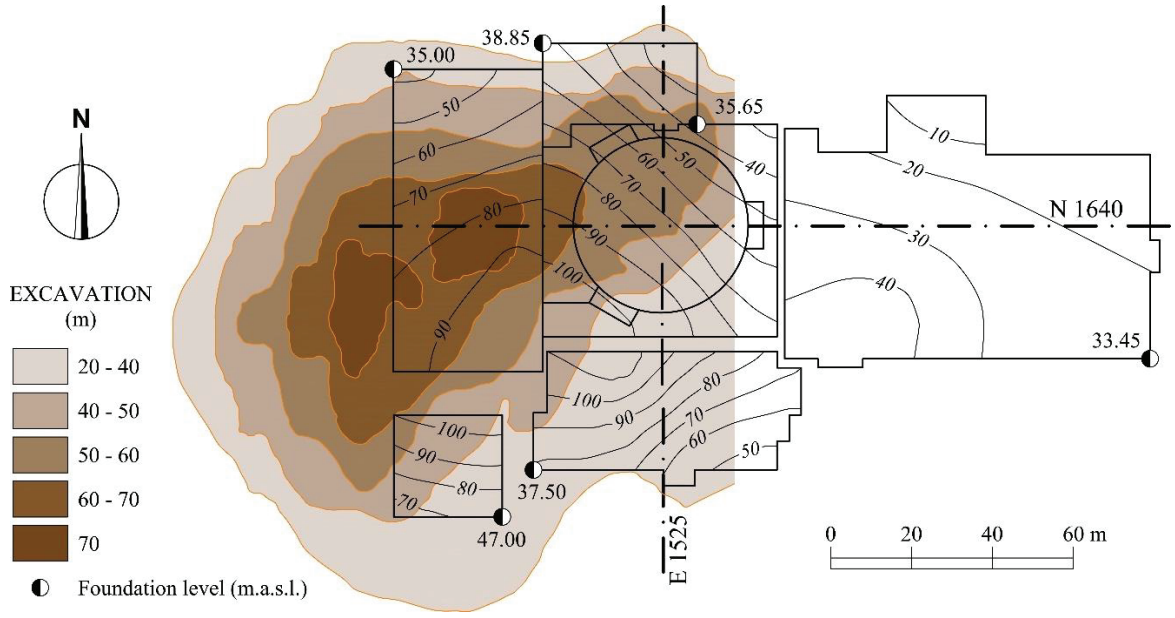

Fig. 3. Heave contours in the period 1979 - 2001.

Other monitoring devices, namely continuous extensometers and vibrating wire piezometers, were very useful to better understand the nature of the observed swelling. The continuous high precision extensometers identified an "active layer" of variable thickness under the buildings (Fig. 4). Measured heave of the buildings was consistent with the accumulated strains measured by the extensometers.

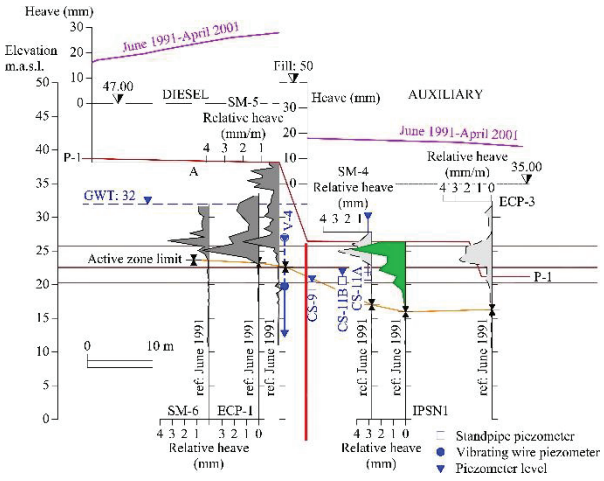

Fig. 4. Active zone under the Diesel and Auxiliary buildings interpreted from strain measurements in continuous extensometers and pore water pressures measured in vibrating wire piezometers. Position indicated (in red) of boring S12 and extensometer IPSN1.

Piezometer's readings added an interesting information. Some of them recorded negative water pressures, an indication of the presence of suction. Some of these negative pressures were measured inside the active layer identified by the extensometers. However, other piezometers showed positive water pressures and, in several cases, the measured piezometric head coincided with the phreatic level mentioned previously.

This information suggested that the large excavation preceding the construction of the power plant damaged the upper levels of the claystone and fissures, most probably horizontal, had developed because of the layered structure of the claystone. The excavation was made by blasting, adding damage to the stress unloading.

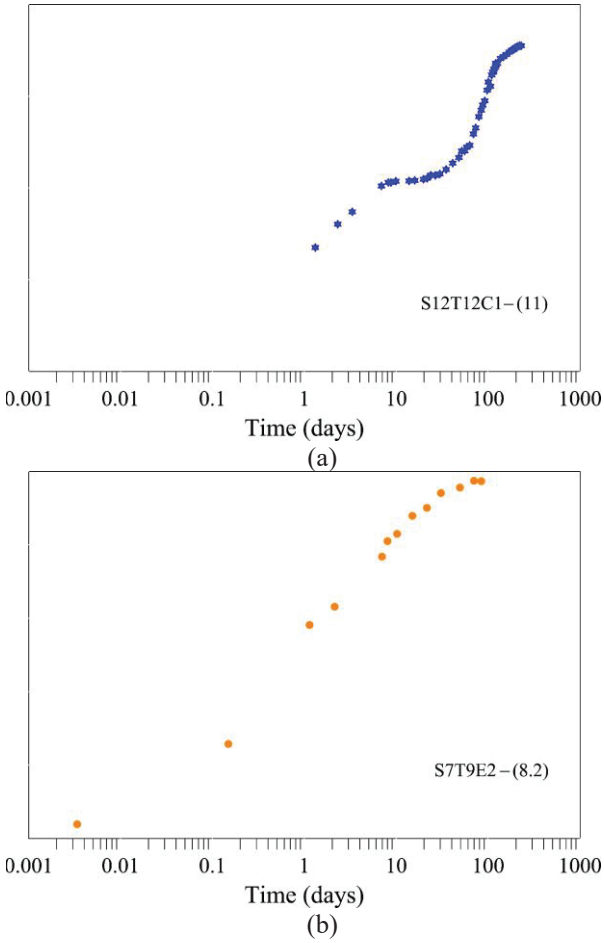

Fig. 5. Long-term oedometer swelling tests. a) Vertical confining stress σ = 0.01 MPa; b) σ = 0.35 MPa.

Long-term swelling tests on samples extracted during boring operations provided additional information ([1], CEDEX, 1988; Fig.5). The plots of

swelling displacements against time, for two vertical confining stresses, show two distinct swelling phases, which may be identified as a primary fast swelling followed by a slow development of secondary swelling. This interpretation led to propose a swelling mechanism which combined two-time scales.

2 A conceptual model for the observed heave

2.1 Basics

Lloret and Alonso [2] published in 1980 a model for the consolidation of unsaturated soils which could reproduce expansion and collapse behaviour. The volumetric constitutive behaviour and the soil permeability were defined by "state surfaces" in terms of confining stress and suction. A finite element program was developed to perform calculations. The application of this model to an oedometer swelling test of a sample of Ascó unsaturated claystone, wetted at the lower face, leads to the heave response shown in Figure 6. The model could not reproduce the "secondary" long-term deformations observed in tests.

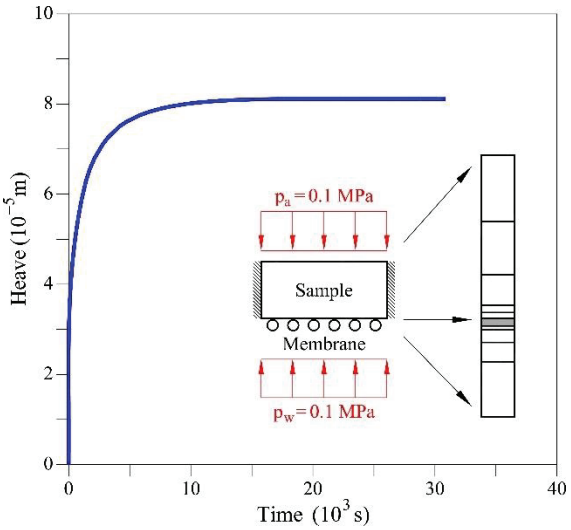

Fig. 6. Computed swelling development of a sample of expansive clay, [3].

Scanning electron images of clay samples began to be published in the 70´s. McGown & Collins [4], described the microstructure of expansive and collapsing soils in terms of the geometrical arrangements of clay particles. They defined concepts such as "elementary particle arrangements", "aggregates" (of elementary particle arrangements) and "intra aggregate" or "inter aggregate" pores. These concepts became familiar for the unsaturated soil research community in the years to follow. The idea to introduce a two-time scale for the development of swelling strains was inspired by these observations. Figure 7 shows a sketch of an idealized structure of the Ascó claystone. Expansive clay units (and other inert grains of the size of silt or sand) define a granular structure. Under unsaturated conditions, capillary menisci at the particle contacts, introduce a set of internal forces attracting the "large" aggregates and grains. The water in menisci is under suction: a "Macro" suction, s_w. A "micro" suction, s_m, is defined inside the clay aggregates. A transfer of water between the aggregates and the macro-pores will establish if s_w and s_m are different. The volumetric deformation of the aggregates could be defined in terms of the micro suction and the prevailing stress. The "macro" arrangement of particles is a second source of deformations in this conceptual model. They could be expressed in terms of the macro suction and the stress. The model was completed by defining the water retention properties of "micro" and "macro" domains.

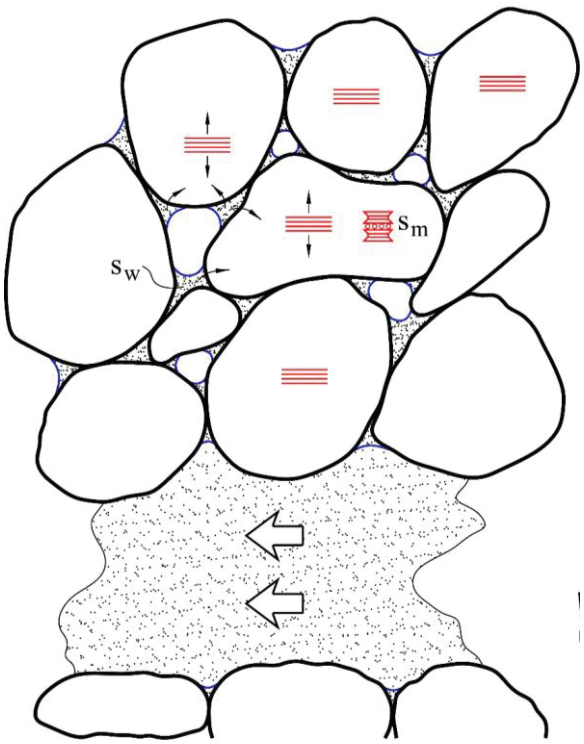

Fig. 7. Representation of clay aggregates in an unsaturated expansive clay and a water-conductive fissure.

These ideas are sketched in Figure 8. A simple elastic representation by means of linear or non-linear expressions for the volumetric deformations and the degree of saturation in terms of the stress variables is suggested in the figure. The key additional component, directly related to the two-time scale of deformations, is the definition of a transfer of water between the macro and micro domains. This is shown in Figure 8 by a linear relationship (coefficient α) between the flow rate between the two structural levels and the difference in micro and macro suctions.

Alonso et al [3] describe the theoretical formulation to solve boundary value problems and its numerical implementation following a finite element methodology. The modified "consolidation" model would hopefully be able to capture the long-term behavior of swelling tests given in Figure 5.

It was found that a dimensionless coefficient,

$$\beta = \frac{\alpha \gamma_w H^2}{k_w^0}$$

that combines coefficient α, the thickness of the sample, H, and the macro permeability, k_w^0, controlled the degree of coupling between the micro and macro deformations [3].

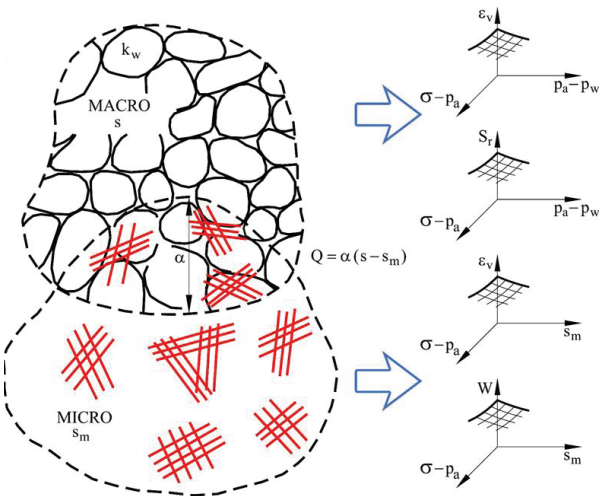

Fig. 8. A continuum representation of two levels of microstructure and a "state surface" approach to define their constitutive behaviour, [3].

This is shown in Figures 9 to 11. A low value, $\beta = 10^{-4}$, (Fig. 9) results in an uncoupling of micro and macro deformations. Micro suction remains essentially constant during the development of macro deformations.

If β increases to $\beta = 10^2$, Figure 10, micro and macro deformations progress at the same rate since the start of the test. In the overall response of the sample it is not possible to distinguish the macro and micro components of deformation. For an intermediate case, $\beta = 10^{-2}$, Figure 11, there is a partial coupling between the two components of deformation.

This model was remarkably accurate to reproduce the available long-term swelling records of Ascó claystone (Fig. 12).

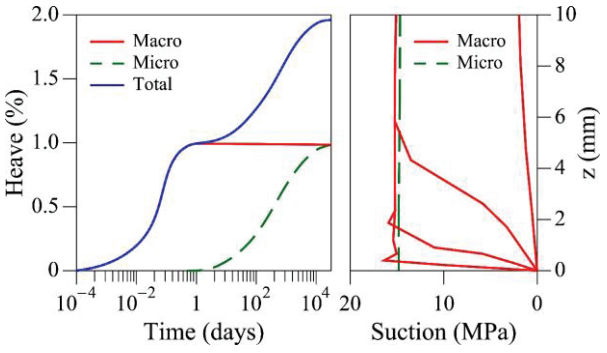

Fig. 9. Modelling a swelling test of a double structure material. $\beta = 10^{-4}$. a) Total strain and strain components; b) Isochrones.

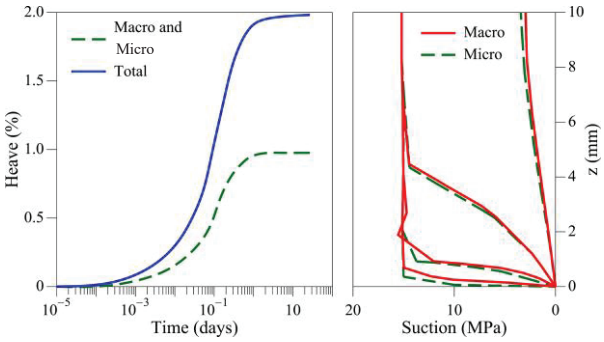

Fig. 10. Modelling a swelling test of a double structure material. $\beta = 10^2$. a) Total strain and strain components; b) Isochrones

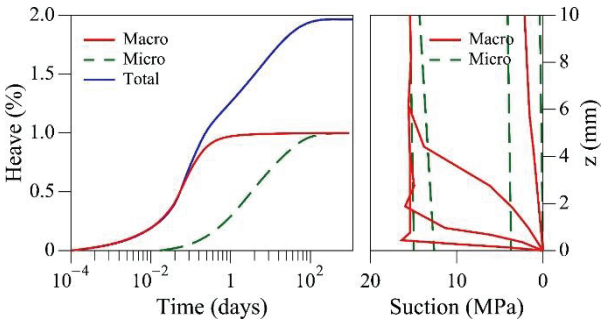

Fig. 11. Modelling a swelling test of a double structure material. $\beta = 10^{-2}$. a) Total strain and strain components; b) Isochrones.

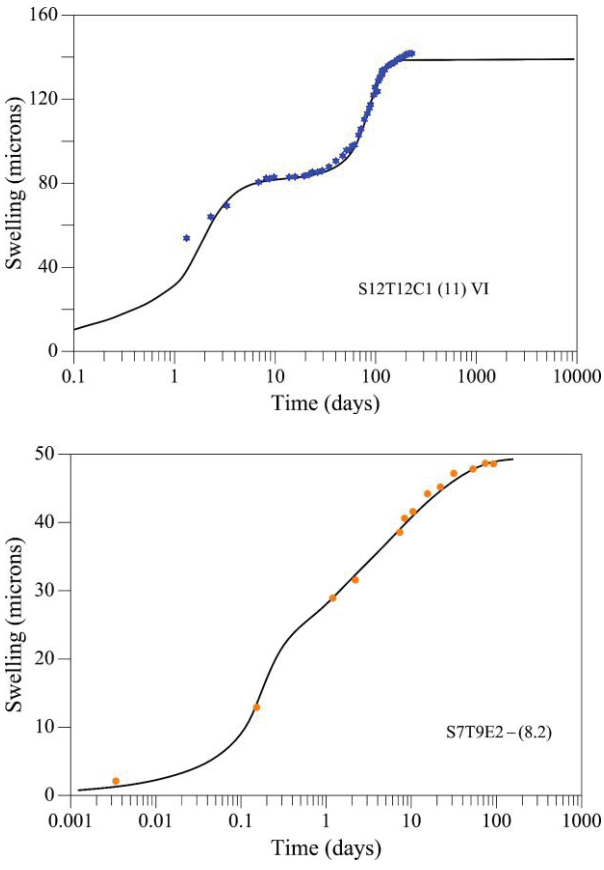

Fig. 12. Comparison of model simulations and test results shown in Figure 5.

2.2 Application to field heave

The active layer under the buildings of the power plant was represented by a set of horizontal open fissures connected to the established phreatic level. The water pressure in fissures followed a hydrostatic law. In between the fissures, the claystone, initially equilibrated under a high estimated suction, s_w = 15MPa, began to expand as the water was progressively wetting the rock. Figure 13 shows a "column" of the claystone at a given location, the position of fissures and the maintained hydrostatic pressure in fissures. Figure 14 shows the calculated isochrones at times t = 0.5 yr. and t = 10 yr., after the beginning of wetting. Micro and macro swelling strains essentially developed simultaneously because of the very low macro permeability of the clay rock.

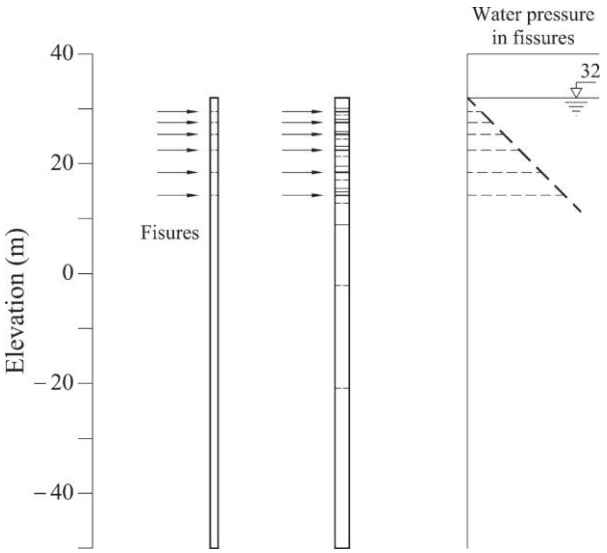

Fig. 13. A column of claystone (5), at a given position in the Power Plant, showing the upper active clay layer and the pressure distribution in fractures. The figure shows the finite element discretization.

Figure 15 shows the calculated heave for the particular position of the calculation column and the heave measurements during a period of 12 yrs. (1977 – 1987). Field swelling records helped to define a set of model parameters for the entire area occupied by the buildings. A good match between model calculations and measurements could be found for a narrow range of claystone saturated permeability around an average value of 2×10^{-13} m/s. The model allows an extrapolation to long times (Figure 15). The prediction is that the rate of heave decreases continuously. 60 yr. after the beginning of the swelling, the heave rate predicted by Figure 15 is close to 1mm/yr.

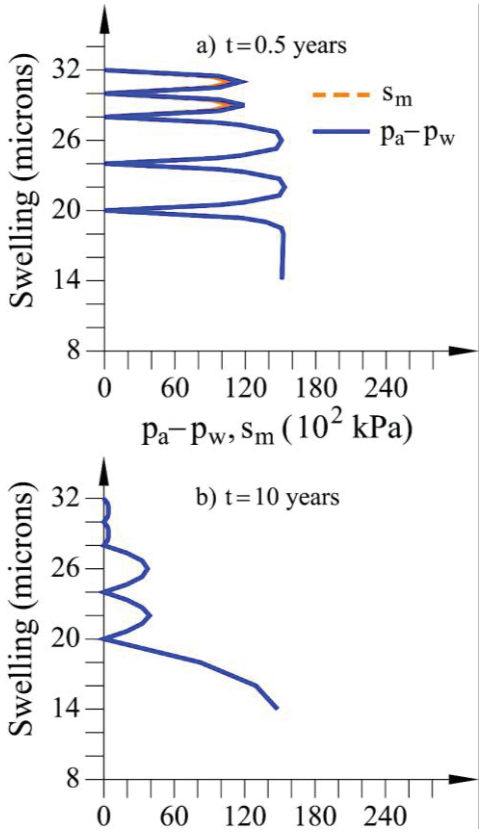

Fig. 14. Suction isochrones at two wetting times for the calculation column shown in Figure 13.

The recorded heave in different locations was analysed, following the outlined methodology. The results were used to produce maps of expected long-term heave distributions. Figure 16 is an example of the predicted heave contours for the period 1980 - 2020.

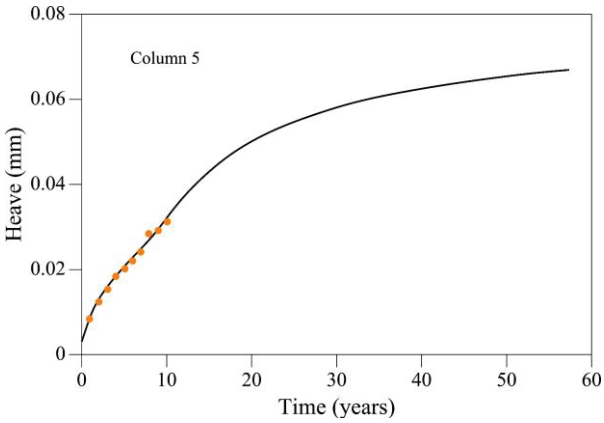

Fig. 15. Measured heave in column 5 and model prediction

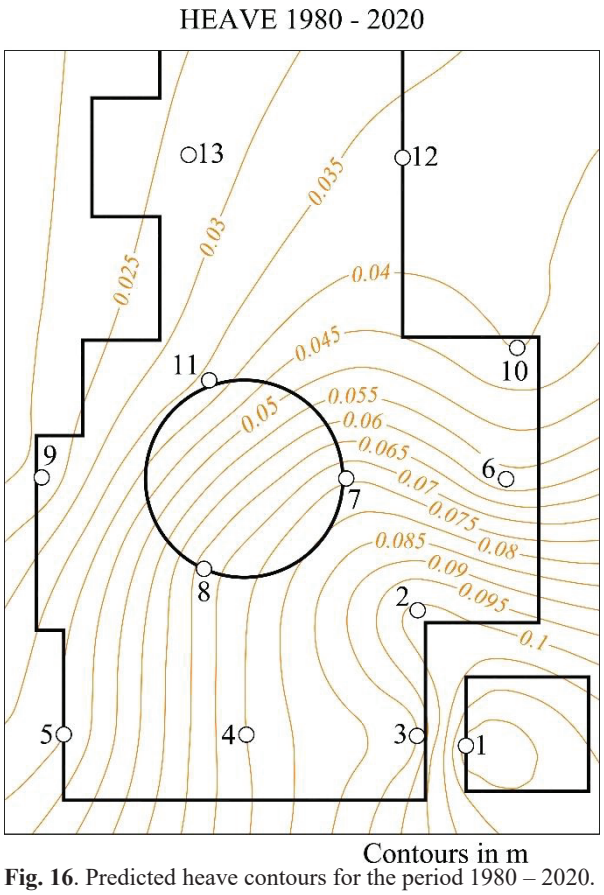

Fig. 16. Predicted heave contours for the period 1980 – 2020.

3 Modelling expansive clays

The work developed to build a model to explain the heave of the nuclear power plant and, even more important for the owners of the plant, to predict the long-term heave, was a very valuable experience to formulate comprehensive models for expansive clays. In 1992 Gens and Alonso, [5], described a framework to explain the behaviour of expansive clays. The core of the proposal is summarized in Figure 17. It shows the yielding surfaces for isotropic stress states in a (p, s) stress plane. The immediate reference for this representation is the BBM for unsaturated soils [6].

The microstructure (aggregates) and the macrostructure are now explicitly recognized in the proposed elastoplastic model. The experience in Ascó suggested that the origin of heave was the swelling of clay aggregates due to wetting. Because of the small distance between clay crystals in aggregates (10 to 100 Å) the aggregates are likely to be saturated in most circumstances. A reference for the aggregate behaviour was the well-established Gouy-Chapman double layer theory. This theory had some implications for the aggregate behaviour: their mechanical response to changes in water suction was reversible and non-linear. The theory is also consistent with the principle of effective stress for saturated soils. Therefore, the volumetric deformation of aggregates against stress and suctions changes was readily formulated. Experimental data also indicated that irreversible volumetric strains may occur as a result of drying (SI yield locus) and wetting (SD yield locus), Figure 17.

It was also recognized that aggregate deformations would modify the macrostructure. This requirement was solved by defining interaction functions (Fig. 18) that allow the calculation of macro strains if the micro strains are known. Interaction functions were properly defined in terms of the current over-consolidation ratio – p/p_0 – where p_0 is the LC-determined yield stress for the current suction [5].

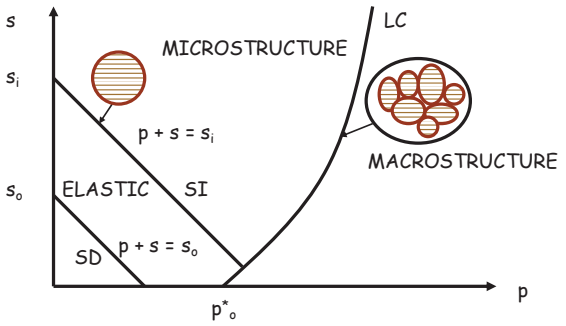

Fig. 17. Yield loci of Barcelona expansive model in a (p, s) plane.

The model was revisited to add more features and it was defined in mathematical terms [7].

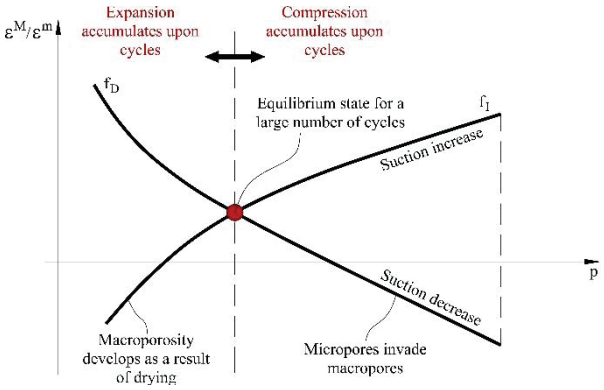

Fig. 18. Interaction functions for suction increase and suction decrease paths.

The double structure representation of the expansive model outlined, also known as BExM, was able to explain a number of observed features of expansive soil behaviour:

- Swelling increases with dry density [5]
- Swelling decreases with confining stress [5]
- Swelling pressure depends essentially on dry density [5]
- Swelling pressure is highly sensitive to stress-suction paths [5]
- Suction cycles: irreversible swelling or shrinkage accumulates [7]
- Effect of wetting rate [8]
- Osmotic effects [9]
- Effects of chemical species [10]
- Long term swelling deformations: this paper

The irony of this successful model, rooted in the ideas developed to explain and predict the heave of the Ascó nuclear plant, is that it was essentially wrong.

4 Is Ascó claystone a double structure expansive material?

Evidence accumulated in the years following the development of the heave model for the nuclear plant strongly suggest that the mechanism of secondary/long term displacements observed in laboratory and in the field was of a different nature. In fact, a review of mineralogical composition of the claystone (5 to 10% of phyllosilicates and a low percentage, (0.8% of the total mineral content) of montmorillonite made it unlikely a microstructure described previously. It was also found that anhydrite was present in percentages ranging from 0 to 30% (average around 10%) and a gypsum content decreasing from 20 – 30% in upper elevations (the references are the borings performed once the site was excavated) to low values at depth. The remaining minerals present are non-active: quartz, carbonates. Esteban [13] performed long term swelling tests on unsaturated samples of compacted Ascó clay powder with and without the addition of anhydrite and found that the delayed "secondary" heave was present only in the clay-anhydrite mixtures.

Sulphated claystone of Eocene age is commonly found in the south-eastern flank of the Ebro basin (Fig.19). Built infrastructure (five tunnels for a high-speed train and a motor way and a large viaduct) built during the past 20 yrs. experienced damage, caused delays and required costly changes in the projects to overcome the rock expansivity. Figure 20 shows a significant case. It refers to a viaduct and it is described in [14] and [15].

Figure 20 shows the massive pile foundation (9 excavated piles 2m diameter, 20 m long) of a viaduct pillar that experienced a sustained heave rate of 5 to 10 mm/month during several years. The profiles of extensometer readings and of anhydrite and gypsum content provide an interesting information: The expansion of the rock, under the pile's tips is related to the presence of anhydrite and not to the presence of gypsum.

Fig. 19. South-east flank of Ebro basin and the location of Ascó power plant and other recently built tunnels and a viaduct.

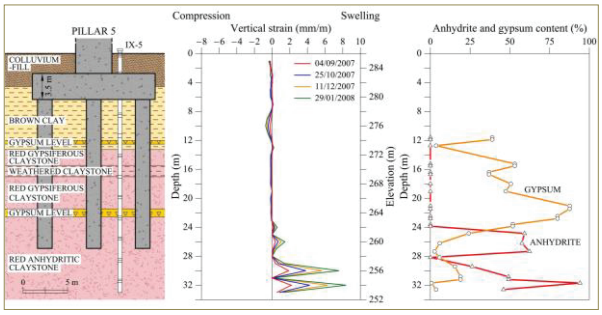

Fig. 20. Pile foundation of a railway viaduct. Extensometer measurements and profiles of anhydrite and gypsum contents in the Eocene claystone.

The next section describes the experience gained to interpret the swelling behaviour observed in sulphated claystones. The answer to the question raised at the beginning of this Section is that the long-term heave observed in the Ascó claystone, in tests and "in situ", is explained by the precipitation of gypsum in discontinuities, provided that the claystone has a noticeable anhydrite content. A short-term expansion is a consequence of a reduction of suction (wetting). Therefore, the concept sketched in Figures 7 and 8 is most probably invalid for Ascó expansive claystone.

5 Long-term expansion of the sulphated claystone

Consider one of the oedometer long-term swelling tests analysed previously. The short-term expansion is essentially a consequence of clay swelling due to wetting. The long-term expansion is now attributed to the precipitation of gypsum in fissures (Figure 21). There is no a clear boundary separating both phenomena but this is not an especial difficulty because the formulation of the model includes the two phenomena since the beginning of a common time. The definition and parameters of the two contributing deformations will define the relative intensity of the two swelling mechanisms.

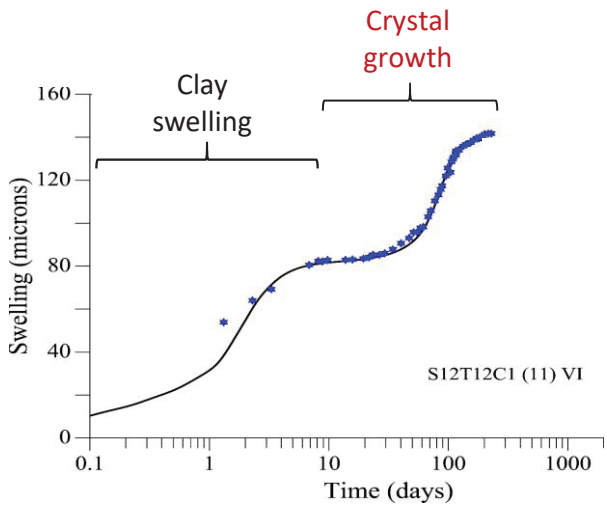

Fig. 21. The two mechanisms contributing to the evolution of claystone swelling in a free oedometer test.

Gypsum precipitates from supersaturated aqueous solutions of calcium sulphate. Supersaturation may be

the result of water evaporation. But there is a second mechanism, very relevant, that does not require evaporation. It only requires the presence of anhydrite. The reason is given in Figure 22. It shows the saturation sulphate concentration of water in contact with anhydrite and gypsum. These equilibrium concentrations depend on temperature. For T = 15ºC, that is a reasonable average temperature of the foundation claystone of Ascó, the equilibrium solute concentration in the presence of anhydrite is 3.2 g/l. In the case of gypsum, it reduces to 2.1 g/l.

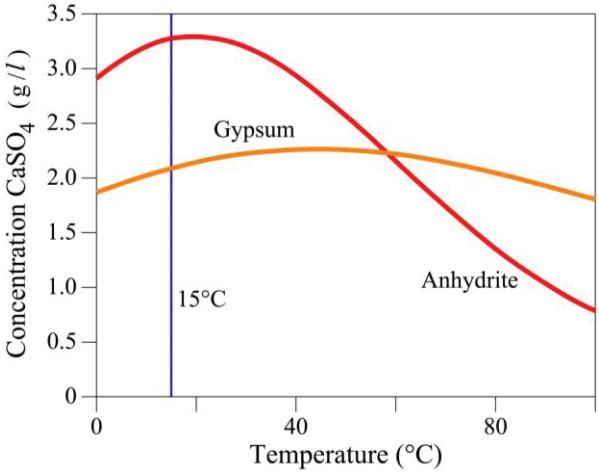

Fig. 22. Equilibrium sulphate concentrations of aqueous solutions in the presence of anhydrite and gypsum.

Consider now the following scenario (Fig. 23). Water flows along a fissure in the claystone. In its path it will find spots where anhydrite is exposed and therefore sulphate will go into solution to a maximum concentration of 3.2 g/l. This solution is supersaturated with respect to gypsum and therefore, the excess of calcium sulphate above the equilibrium concentration for gypsum will tend to precipitate. This process will be facilitated if gypsum crystals are also found in the path of the flowing water. Strictly speaking, this process does not require water flow because a diffusion of ions caused by a gradient of sulphate concentrations will also lead to gypsum precipitation.

Crystal growth in a confined volume (the fissure or big enough void) will generate a force against the confinement wall and probably an expansion of the claystone. The crystal growth-induced swelling pressure is analysed below.

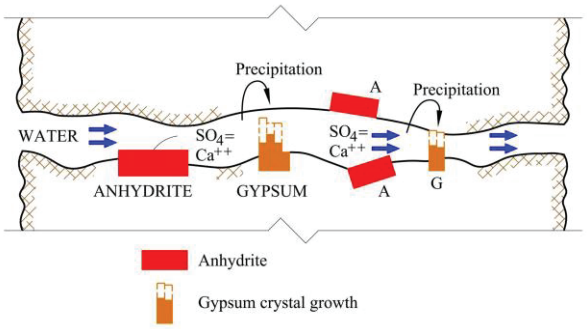

Fig. 23. Sketch to illustrate the dissolution of anhydrite and precipitation of gypsum in a water saturated fissure in the claystone.

Modelling the outlined phenomena at a large scale will require the formulation of balance equations for solid, water and air, momentum balance (equilibrium), energy balance, if temperature changes are required and constitutive equations. This is the standard framework to deal with coupled thermo-hydro-mechanical phenomena in porous media. However, there are some specific characteristics of the problem that will be described in more detail.

5.1 Mass balance of the solid phase

Figure 24 shows a phase diagram of the sulphated claystone. The volumetric ratios of anhydrite and gypsum are differentiated from the rest of solid (inert) minerals because they may dissolve or precipitate.

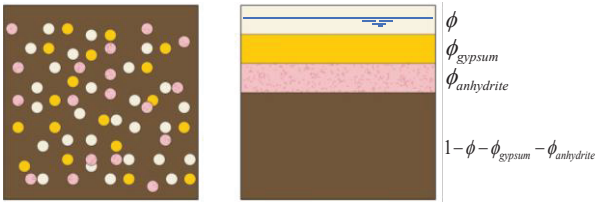

Fig. 24. Phase diagram of an unsaturated sulphated claystone.

The equations of mass balance of insoluble and soluble minerals read as follows:

$$\frac{\partial}{\partial t}\left(\rho_s\left(1-\phi-\phi_{anh}-\phi_{gyp}\right)\right)+\nabla\cdot\left[\left(\rho_s\left(1-\phi-\phi_{anh}-\phi_{gyp}\right)\right)\frac{d\boldsymbol{u}}{dt}\right]=0 \quad (1)$$

$$\frac{\partial(\rho_{gyp}\phi_{gyp})}{\partial t}+\nabla\cdot\left[\left(\rho_{gyp}\phi_{gyp}\right)\frac{d\boldsymbol{u}}{dt}\right]=\frac{dm_{gyp}}{dt} \quad (2)$$

$$\frac{\partial(\rho_{anh}\phi_{anh})}{\partial t}+\nabla\cdot\left[\left(\rho_{anh}\phi_{anh}\right)\frac{d\boldsymbol{u}}{dt}\right]=\frac{dm_{anh}}{dt} \quad (3)$$

where **u** is the displacement vector. If ρ_s, ρ_{gyp}, ρ_{anh} are constant, combining equations and re-arranging terms leads to:

$$\frac{D_s\phi}{Dt}=[(1-\phi)]\nabla\cdot\frac{d\boldsymbol{u}}{dt}-\frac{1}{\rho_{gyp}}\frac{dm_{gyp}}{dt}-\frac{1}{\rho_{anh}}\frac{dm_{anh}}{dt} \quad (4)$$

This equation expresses that the rate of change of porosity of the claystone is found by subtracting the rates of anhydrite and gypsum masses dissolution or precipitation from the volumetric strains due to global deformation. The rates of mass dissolution or precipitations are described by “kinetic equations”.

5.2 Kinetic equations for dissolution-precipitation

Kinetic equations predict the dissolution or precipitation in terms of several variables: the volumetric fraction of the salt (porosity: ϕ_{anh} *or* ϕ_{gyp}), its specific surface (σ_c: m^2/m^3) and the mass fraction of dissolved mass of salt in water, ω_l^m. ($\rho_l\omega_l^m$ is the concentration in units of mass/volume). However, the literature offers several mathematical expressions. Here we adopt the proposal of Lasaga [16]. The kinetic equation for gypsum is:

$$\frac{dm_{gyp}}{dt} = \sigma_c \kappa \xi \phi_{gyp} \left(\left| \left(\frac{\omega_l^m}{\omega_{sat,gyp}{}_l^m(T,p')} \right)^\theta - 1 \right| \right)^\eta$$
$$\xi = \frac{\omega_l^m - \omega_{sat,gyp}{}_l^m}{\left|\omega_l^m - \omega_{sat,gyp}{}_l^m\right|} \quad (5)$$

In this expression κ is a rate constant and ξ is a number (+1 or -1) to describe dissolution or precipitation. The saturation concentration, following Scherer [17]:

$$\omega_{sat,gyp}{}_l^m = \omega_0{}_{l,sat,gyp}^m \, exp\left(\frac{p' v_c}{R_g T}\right) \quad (6)$$

depends on the confining stress, p', the molar volume of gypsum, v_c , and the absolute temperature, T. $\omega_0{}_{l,sat,gyp}^m$ is the equilibrium concentration for an unloaded crystal. A quadratic law ($\theta = 1;\ \eta = 2$) is consistent with experimental results reported in [18] and it was adopted in this work. The product $\sigma_c \kappa$ is a "compound kinetic coefficient" that may be determined in swelling experiments.
A similar expression holds for the anhydrite. The kinetic equations enter in the transport equation for the sulphate concentration as sink or source terms.

5.3 Strains induced by gypsum precipitation

The simple rule,

$$\frac{d\varepsilon_i}{dt} = \frac{\gamma_i}{\rho_{gyp}} \frac{dm_{gyp}}{dt}\ ,\ i = 1,2,3 \quad (7)$$

provides the rate of strain expansions in direction *i*. It is accepted that stress will also control the development of precipitation-induced strains as follows [18]:

$$\gamma_i = \gamma_{max} e^{-b\sigma'_i} \quad (8)$$

Experiments, [19], [20] in sulphated rock provide a validation for this approach.

5.4 Fractures

Crystals grow in rock fractures. In fact, crystals need a certain empty space to grow initially. Crystals growing in a dense claystone matrix have not been observed. Fractures may be pre-existent or a result of engineering works. In the case of Ascó power plant, the deep excavation performed by successive blasting is probably the origin of horizontal fissures observed in the horizontally layered stiff and dense sulphated claystone. The propagation of fissures and fractures may be also a consequence of crystal growth in existing fissures or damaged surfaces. The experience in the laboratory and in the field is that crystal growth increases the thickness of fissures, damages the rock (loss of strength, reduction of specific weight) and increases the water conductivity. The last point may be quantified under certain simplified assumptions (Figure 25) [21]: In a set of parallel fractures of width b that experiences a normal strain ε, the updated b value is:

$$b_{new} = b_{initial} + s(\varepsilon - \varepsilon_0) \quad (9a)$$

where s is a reference distance (for instance, the spacing between layers) and ε_0 is an initial deformation. The intrinsic permeability of the fracture in a laminar flow (Poiseuille) will be:

$$k_{fracture} = \frac{b2}{12} \quad (9b)$$

The equivalent permeability of the medium (fractured claystone):

$$k = k_{porous\ matrix}\left(1 - \frac{b}{s}\right) + k_{fracture}\frac{b}{s}$$
$$\cong k_{porous\ matrix} + \frac{\left(b_{initial} + s(\varepsilon - \varepsilon_0)\right)^3}{12s} \quad (10)$$

is dominated by the permeability of fractures.

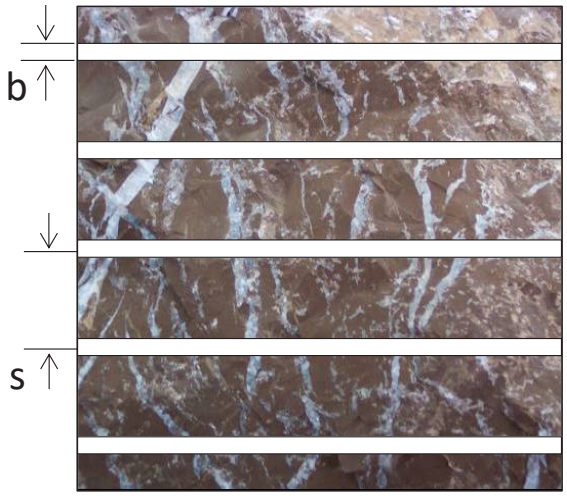

Fig. 25. Geometry of parallel fractures in the claystone

5.5 Crystal growth and swelling pressure

The dissolution or precipitation of a crystal in an aqueous solution is determined by the chemical potentials of the crystal, μ_c, and the solution, μ_s.

If $\mu_c < \mu_s$ crystal will grow until $\mu_c = \mu_s$. If $\mu_c > \mu_s$ crystal will dissolve until $\mu_c = \mu_s$. The chemical potentials of crystal and solute are given by [17], [22]:

$$\mu_c = \mu_{c,0} + v_c(p_c - p_{c,ref}) \quad (11)$$

$$\mu_s = \mu_{s,0} + R_g T \ln a_s \quad (12)$$

where p_c is the pressure applied to the crystal, a_s is the activity (effective concentration) of the solution, v_c is the molar volume of crystal and $R_g$is the ideal gas constant.

Consider, Figure 26, a crystal immersed in a solution at a (liquid) pressure p_l. The crystal will be in equilibrium (no dissolution, no growth) if the chemical potentials $\mu_c = \mu_s$. This is achieved if a pressure p_c,

$$p_c = p_l + \frac{R_g T}{v_c} ln\left(\frac{a}{a_0}\right) \quad (13)$$

is applied to the crystal. In (13), p_l is the pressure of the liquid solution of the reference state, a_0 is the activity of the solution at the reference state, p_c is the pressure applied to the crystal and a is the current activity of the solution.

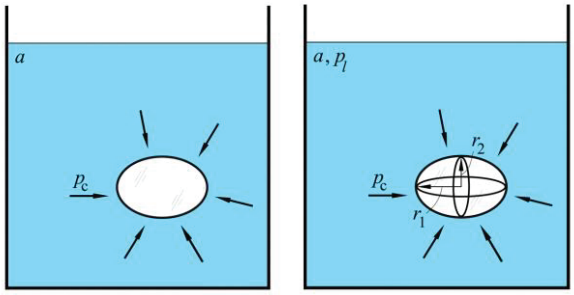

Fig. 26. A crystal submerged in an aqueous solution of activity *a* (left) and the same crystal under a pressure p_c to prevent crystal growth (right).

Consider now the interfacial energy, γ_{cl}, at the boundary crystal-solution. Following Laplace, the pressure experienced by a crystal surface in contact to a liquid, due to its curvature ($1/r_1 + 1/r_2$), is

$$p_c = p_l + \gamma_{cl}\left(\frac{1}{r_1} + \frac{1}{r_2}\right) \tag{14}$$

For consistency,

$$p_c - p_l = \gamma_{cl}\left(\frac{1}{r_1} + \frac{1}{r_2}\right) = \frac{R_g T}{v_c} ln\left(\frac{a}{a_0}\right) \tag{15}$$

Figure 27 shows a cylindrical crystal, in a supersaturated solution of activity *a*, growing against a cylindrical wall (a fissure in the claystone). The thin contact volume is assumed to maintain the activity of the aqueous solution in the fissure.

The rigid fissure wall is applying a pressure, p_d, to prevent the crystal growth. The crystal has a curvature $1/r_1 + 1/r_2 = 2/r$ in the spherical caps and $1/r_1 + 1/r_2 = 1/r + 0 = 1/r$ in the cylindrical surface.

Since the solution activity is the same in a and b, the crystal pressures are equal, $p_{c,a} = p_{c,b}$. Following Laplace (equation 14) $p_{c,a} - p_l = \gamma_{cl}(2/r)$ in the spherical cap and $p_{c,b} - (p_l + p_d) = \gamma_{cl}(1/r)$. Therefore, the pressure of the crystal against the cylindrical wall is

$$p_d = \frac{\gamma_{cl}}{r} = \frac{R_g T}{2v_c} \ln\left(\frac{a}{a_0}\right) \tag{16}$$

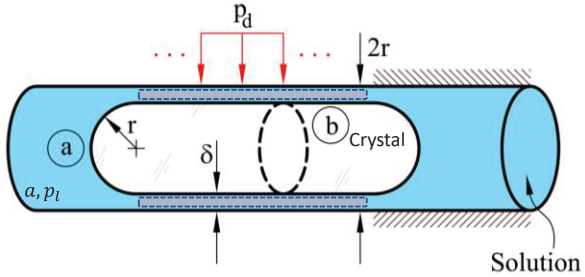

Fig. 27. A cylindrical crystal, limited by spherical caps, growing in a cylindrical fracture, saturated with a sulphated solution of activity *a*.

For the equilibrium activities of anhydrite and gypsum, the gypsum crystal pressure in the configuration of Figure 27 is:

$$p_d = \frac{1}{2}\frac{R_g T}{\mathrm{v}_{c,gypsum}} \ln\frac{a_{anhydrite}}{a_{gypsum}} =$$

$$= \frac{1}{2}\frac{8.31\,\frac{\mathrm{cm^3 MPa}}{\mathrm{K\,mol}} \cdot 298.15\ \mathrm{K}}{74.69\,\frac{\mathrm{cm^3}}{\mathrm{mol}}} \ln\frac{10^{-4.36}}{10^{-4.58}} = 8.40\mathrm{MPa} \tag{17}$$

This is a high value if compared with swelling pressures of expansive clays and claystones. Despite the approximations and hypothesis introduced in the derivation of (17), the result indicates that the anhydrite-gypsum transformation through a solution-precipitation mechanism will be a serious problem in excavations and foundations in anhydritic claystones.

Summarizing, the model developed to analyze boundary value problems involving flow and deformation in anhydritic claystones, requires the solution of the following equations:

- Solid balance equation (two soluble species + one insoluble)
- Water mass balance equation (sink/source terms from dissolution/precipitation)
- Equilibrium (imposed swelling deformations from precipitated gypsum)
- Solute mass conservation equation (for the calcium sulphate)
- Development of fractures
- Constitutive relations

This formulation was included in the Finite Element THMC computer program "Code Bright" [24].

6 Modelling the power plant heave

The first step was to apply the model developed for the sulphated claystone to reproduce long-term swelling tests with the purpose of a) Validating the proposed framework and b) Identifying some constitutive parameters. However, tests on small samples are a rough estimate of real scale conditions, especially when facing a heterogeneous formation.

The primary, clay-swelling related swelling, was of secondary importance for the long-term heave. For the one-dimensional conditions of the oedometer tests performed, the nonlinear elastic equation,

$$\frac{\Delta e}{1+e} = a_1 \Delta \ln(p) + a_2\, \Delta \ln\left(\frac{s+\mathrm{patm}}{\mathrm{patm}}\right) \tag{18}$$

describes the volumetric deformation in terms of changes in mean stress and suction.

Figure 28 shows the swelling displacements measured in a free swelling test (sample dimensions 70 x 20 mm). The sample was initially unsaturated: w_0 = 1.25%; e_0 = 0.12; S_r = 0.25; s = 190 MPa. The volumetric fractions of anhydrite and gypsum are $\phi_{anh} = 12\%, \phi_{gyp} = 16\%$. At the start of wetting, distilled water, at zero pressure, was put in contact with the lower face of the sample. The oedometer was covered by a Perspex lid to isolate the test. At the end of

the swelling period the sample was loaded and unloaded. Water flow was characterized by an intrinsic saturated permeability (K = 10^{-21} m^2, a relative permeability (S_r^3) and a laboratory-determined Van Genuchten water retention relationship:

$$S_r = \left[1 + \left(\frac{s}{p_0}\right)^{\frac{1}{1-\lambda}}\right]^{-\lambda} \quad (19)$$

where λ =0.45 and p_0 = 36 MPa.

The following parameters: a_1 = 9x10^{-3}, a_2 = -5.2x10^{-4} and a compound kinetic coefficient, $\sigma_c\kappa = 10^{-6}$, led to a very good agreement with the measurements (Figure 28). This exercise was repeated for other swelling tests under different confining stresses. A preliminary set of model parameters could be found.

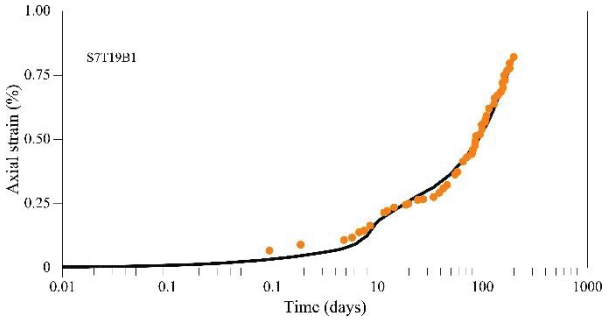

Fig. 28. Free swelling long-term swelling test of a sample of Ascó marl and model performance. $\phi_{anh} = 0.12$; $\phi_{gyp} = 0.16$.

Figure 29 shows a reasonable approximation of the thickness of the active zone. Continuous extensometer data, extending several years, were helpful to approximate the lower boundary of the damaged claystone.

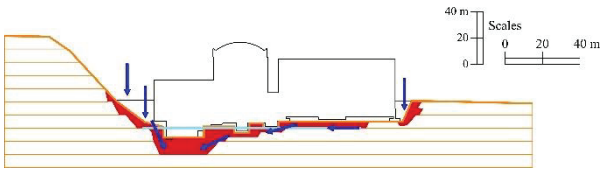

Fig. 29. Central cross section of the plant showing the estimated thickness of the active swelling layer and water flow.

Figure 39 shows also the access of rainfall water to the damaged claystone. It was a consequence of the difficult drainage of the excavated geometry to place the buildings.

Figure 4 shows the position of extensometer IPSN1. This extensometer was particularly interesting because it provided a long-term record (10 yr.) of swelling deformations (Fig. 30). The pattern of deformations repeats over the years and the peak deformations suggests that three damaged zones could explain the position of gypsum precipitation. The analysis described here is restricted to a one-dimensional column

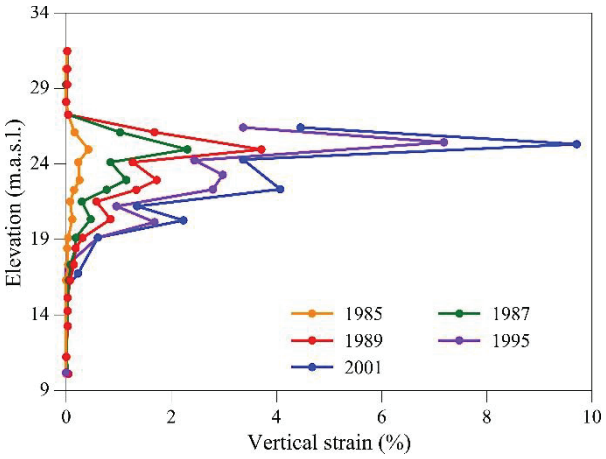

Fig. 30. Vertical profile of swelling deformations measured in extensometer IPSN1

The nearest boring to IPSN1 extensometer is S12 (Fig. 4). Figure 31 shows the volumetric fractions of anhydrite. A constant volume fraction of 0.15 was adopted for the swelling simulation

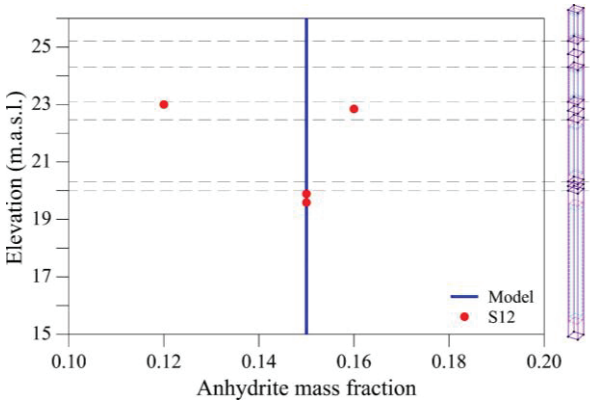

Fig. 31. Anhydrite volumetric fraction determined in samples recovered in boring S-12.

A procedure to calculate the evolution of fracture opening was built into the entire column. The basics were given above (Equation 9a).

The claystone capillary swelling due to wetting was characterized by a_1 = *9x10^{-3}*, a_2 = *-4x10^{-4}* (equation 18). These parameters were estimated from the modelling of swelling tests. Hydraulic parameters derive also from the simulation of swelling The compound kinetic coefficient, $\sigma_c\kappa = 7.5e-7\frac{kg}{m3s}$, was also close to the value derived from tests on specimens. The capillary swelling expansion had a very limited effect on the observed field heave, that was dominated by gypsum precipitation. Figure 32 shows a good agreement between model prediction and extensometer readings.

Figure 33 shows the model prediction of heave, applied to conditions of the boring S-12, and a few surface heave records measured in points located in the vicinity of S-12.

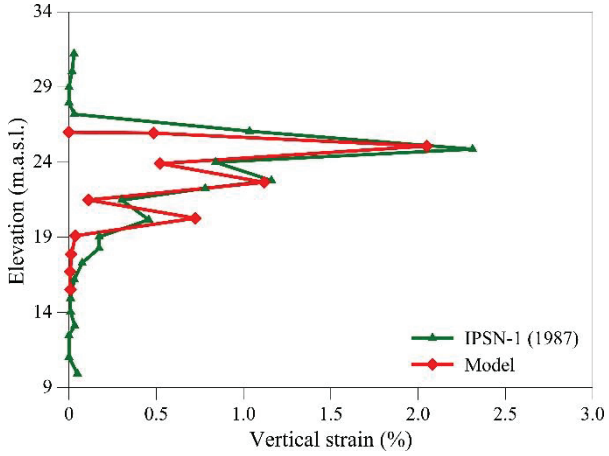

Fig. 32. Comparison between IPSN-1 extensometer deformations in 1987 and model predictions.

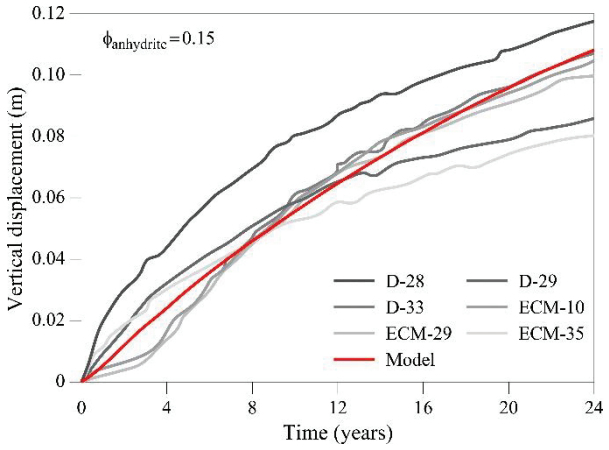

Fig. 33. Model predictions for the conditions estimated in borehole S-12 and measured heave records in neighbouring locations. Initial volumetric fraction of anhydrite, ϕ_{anh} = 0.15.

The model, for $\phi_{anh} = 0.15$, predicts heave rates somewhat higher than measured ones at the end of the calculation period (24 yr.). Significant parameters to control the long-term heave are the initial volumetric fractions of anhydrite (specially) and gypsum.

Because of the observed spatial heterogeneity of sulphated minerals in the claystone it is logical to accept a certain error in predictions.

7 Summary and conclusions

The paper describes a long involvement to understand and to develop predicting models for the observed heave of a nuclear power station ever since the conclusion of building´s construction in 1977. The maintained heave rate over long periods of time and the pattern of long-term swelling tests fixed the attention in the nature of a "secondary" expansion. Advances in understanding expansive clay microstructure suggested initially that a water transfer between micro and macro clay structures could explain laboratory results. The resulting model proved to be very flexible and accurate to reproduce experiments. It was then applied to reproduce observed heave records and it was also useful for long-term heave predictions.

This double structure expansive clay model was later extended, within a more general framework, to a constitutive model that proved to be useful to interpret and reproduce several features of expansive soil behaviour, listed in the text.

However, this interpretation of the observed heave overlooked the significant contents of anhydrite and gypsum in the claystone. In the years to follow the modelling of Ascó power plant heave, several infrastructures (tunnels, viaduct) built in the similar geological formation of Ascó, experienced severe short and long-term deformations and high swelling pressures that were interpreted by a different mechanism: the precipitation of gypsum crystals in fractures and discontinuities of the claystone from supersaturated water in calcium sulphate. The presence of anhydrite explains the supersaturation. The subsequent research led to the formulation of a hydro-mechanical and chemical model that was capable of explaining field behaviour in qualitative and quantitative terms.

The Ascó case was revisited here from a new alternative explanation of the physics of the observed heave. Precision extensometers detected the presence of bands of claystone expansion whose origin is associated with the damage created by the excavation.

A key component of the model developed are the kinetic expressions to determine the rate of dissolution of anhydrite and the rate of accumulation of precipitated mass of gypsum. The gypsum crystallization rate increases with the concentration of sulphates in water, and the concentration of solid gypsum and decreases with applied effective pressure. A relationship between mass of precipitation and induced deformations, that depends also on effective stress, is given. The crystal - growth model, if compared with the initial double structure clay model, is also accurate to describe the available long-term swelling tests. This is not a surprise because it is a relatively complex model that incorporates a high number of parameters, if compared with the clay model. However, it is believed that it provides a closer interpretation to the actual swelling mechanisms.

The performance of the new model at field scale is quite satisfactory, especially because of the highly heterogenous spatial distribution of gypsum and anhydrite contents. The observed reduction of heave rate with time is shown to be a consequence of the dissolution of anhydrite. The heave will theoretically stop when all the anhydrite content in the damaged and water saturated claystone bands is exhausted by dissolution.

Acknowledgements

The first part of this paper, dealing with the double structure clay model, was a "joint venture" with the author's colleagues, Professors Antonio Gens and Antonio Lloret. It was a very stimulating and enjoyable research period that ended up in a forecasting of the

long- term expected heave of the power station. My deep thanks and appreciation to them.

Years later, the observations and increasing understanding of the heave observed in viaducts and tunnels founded and excavated in sulphated clay-stones, similar to the rock foundation of the nuclear power plant, led to the revision of the heaving mechanism. The work described here is the result of a maintained effort, during the past two decades, of several researchers: the late Dr. Iván Berdugo, Prof. Luciano Oldecop, Prof. Sebastià Olivella and, specially, Assistant Professor Anna Ramon. Their contribution is greatly acknowledged. During the preparation of this lecture the author was very fortunate to receive the help and dedication of Ass. Prof. Anna Ramon, Assoc. Prof. Núria M. Pinyol and, specially, Eng. Mateu Maglia. My gratitude to all of them.

References

1. CEDEX Análisis de los resultados de los ensayos de laboratorio de las etapas 7 y 12, encaminados al estudio para la mejor comprensión de los fenómenos de hinchamiento de las margas del subsuelo en la Central Nuclear de Ascó II. Informe Parcial. Tomo único- Clave: CEDEX - 32-513-5-0-15. Madrid (1988).
2. A. Lloret, E. E. Alonso, Géotechnique, **30**, 4, 449 – 477 (1980)
3. E. E. Alonso, A. Gens, A. Lloret, Computer Methods and Advances in Geomechanics, Beer, Booker &Carter (eds). Balkema (1991)
4. A. McGown, K. Collins, Proc. 5th Pan Am. Conf. on SMFE. **1**: 325 – 332. Buenos Aires. (1975)
5. A. Gens, E. E. Alonso, Canadian Geotechnical Journal, **29**, 4, 1013-1032 (1992)
6. E. E. Alonso, A. Gens, A. Josa, Géotechnique, **40**, 3, 405-430 (1990)
7. E. E. Alonso, J. Vaunat, A. Gens, Engineering Geology, **54**, 1-2, 173-183 (1999)
8. E. E. Alonso, N. M. Pinyol, C. Hoffmann, Proc. of the 6th International Conference on Unsaturated Soils, UNSAT, pp. 15-29. Sydney (2014)
9. E. E. Alonso, Proc. of the 2nd International Conference on Unsaturated Soils. Beijing. International Academic Publishers, **2**, 37-70 (1998)
10. L. do N. Guimaraes, A. Gens, M. Sánchez, S. Olivella, Géotechnique, **63**, 3, 221-234 (2013)
11. E. E. Alonso, I. R Berdugo, A. Ramon, Géotechnique, **63**, 7, 584–612 (2013)
12. J. A. Pineda, E. E. Alonso, E. Romero, (2014). Géotechnique, 64, 1, 64–82 (2014)
13. F. Esteban, Doctoral dissertation. Universidad de Cantabria. Spain. (1990)
14. E. E. Alonso, A. Ramon, Géotechnique, 63, 9, 707–719 (2013)
15. A. Ramon, E. E. Alonso, Géotechnique, 63, 9, 720–732 (2013)
16. A. C. Lasaga, J. Geophys. Res. **89**, B6, 4009–4025 (1984)
17. G. W. Scherer, Cement and Concrete Research, **29**, 1347-1358 (1999)
18. L. Oldecop, E. E. Alonso, Int. J. Rock Mech. & Min. Sci., **54**: 90–102 (2012)
19. T. Huber, E. Pimentel, G. Anagnostou Energy Procedia **76**, 87–95. (2015)
20. A. Ramon, E. E. Alonso, S. Olivella, Géotechnique, 67, 11, 968-982 (2017)
21. S. Olivella, E.E. Alonso, Géotechnique, **58**, 3, 157-176 (2008)
22. D. Langmuir, Aqueous environmental geochemistry. Upper Saddle River: Prentice Hall (1997)
23. G. W. Scherer, Stress from crystallization of salt in pores. In Proc. *9th* Int. Cong. Deterioration and Conservation of Stone. Amsterdam: V. Fassina. (2002)
24. https://deca.upc.edu/en/projects/code_bright